IEEE Open Journal of
Antennas and Propagation

Received 23 July 2020; revised 16 September 2020; accepted 28 September 2020. Date of publication 1 October 2020; date of current version 19 October 2020.

Digital Object Identifier 10.1109/OJAP.2020.3028297

An Accurate Equivalent Circuit Model of Metasurface-Based Wireless Power Transfer Systems

DANILO BRIZI [1,2] (Member, IEEE), NUNZIA FONTANA [3] (Member, IEEE), SAMI BARMADA [3] (Senior Member, IEEE), AND AGOSTINO MONORCHIO [1,2] (Fellow, IEEE)

[1]Department of Information Engineering, University of Pisa, 56122 Pisa, Italy

[2]Consorzio Nazionale Interuniversitario per le Telecomunicazioni, 43124 Parma, Italy

[3]Department of Energy, Systems, Territory and Construction Engineering, University of Pisa, 56122 Pisa, Italy

CORRESPONDING AUTHOR: D. BRIZI (e-mail: danilo.brizi@ing.unipi.it)

ABSTRACT In this article, we introduce a general analytical procedure to unambiguously characterize a metasurface through its lumped circuital equivalent in resonant inductive Wireless Power Transfer (WPT) applications. The proposed model incorporates the finite extent of the slab, as well as the WPT near field operative regime and the presence of the particular driving/receiving coils arrangement, providing quantitative and easy-to-handle parameters which can be manipulated to achieve WPT performance enhancement. We first develop the theoretical background aimed at the lumped parameters extraction, which reveals, for WPT applications, more accurate and robust with respect to the conventional sub-wavelength homogenization theories based on infinite slab extent and impinging plane wave hypotheses. We provide some general guidelines for the design of metasurfaces for WPT performance enhancement based on the derived circuit model; afterwards, we numerically design a test-case consisting of two resonant coils (driver and receiver, respectively) with an interposed passive metasurface to verify the developed theory. Finally, we show some measurements performed on a fabricated prototype, that present an overall excellent agreement with both the lumped model and the numerical simulations.

INDEX TERMS Metamaterial, metasurface, wireless power transfer, equivalent circuit, resonant coils.

I. INTRODUCTION

METAMATERIALS and their 2D counterparts (i.e., metasurfaces) represent nowadays a well-established and important research field in the electromagnetism community [1], [2]. Their capability to show dielectric and magnetic properties not found in nature have been proved to be extremely useful in a number of different applications. In particular, they can provide negative values of dielectric permittivity and magnetic permeability, with isotropic or even anisotropic characteristics when properly designed [3]–[8]. The basic structure usually consists in a 2D or 3D array of resonant unit-cells; indeed, the resonant properties of the unit-cells are responsible of the exotic dielectric permittivity and magnetic permeability [9]–[11]. In addition, to properly work, one fundamental requirement relies in the unit-cell dimension, which must be in the extremely subwavelength regime. In this way, the electromagnetic field impinging in the meta-structure cannot distinguish its elementary organization and it is interpreted as a homogeneous material [12]–[15].

Among the numerous applications, resonant inductive Wireless Power Transfer is one of the most stimulating field in which metamaterials and metasurfaces can be employed [16]–[18]. The rapidly increasing interest in transferring energy wirelessly to remove any type of transmission line from electronic devices makes research on WPT an extremely hot topic. In such applications, the control on the magnetic permeability is crucial for enhancing the magnetic field produced by the driving coil, which is responsible of the induced useful current at the receiver. In the literature, an impressive effort has been directed to exploit metamaterials and metasurfaces in WPT, continuously improving their

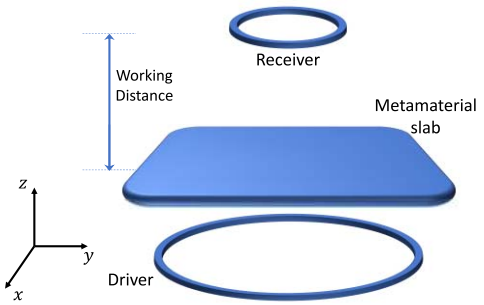

FIGURE 1. Pictorial representation of a typical WPT arrangement in the presence of a metasurface.

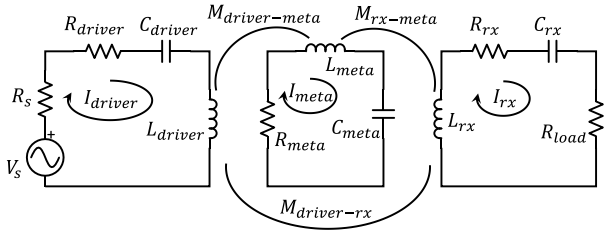

FIGURE 2. Lumped elements representation of the WPT arrangement constituted by a resonant driver and receiver and the meta-structure *RLC* equivalent.

performance and reducing their size. Several works have shown that a negative permeability can enhance magnetic evanescent waves [19]–[22], thus increasing WPT efficiency. Moreover, planar resonators and wires in different arrangements are very popular: it has been demonstrated that spiral resonators, split rings, in a single or double layer configuration are able to improve the efficiency of the inductive link [23]–[33]. Other studies have explored the possibility to reduce the electric field amplitude through resonators' arrays for safety purposes [34].

As a matter of fact, metamaterials and metasurfaces design is usually performed following the classical electromagnetic theory [22], where the slab is considered infinite in extent and a plane wave is impinging upon it. Starting from the single unit-cell conception, periodic boundary conditions are successively applied to retrieve the electromagnetic properties of the infinite slab [35]; often, several iterations optimizing the unit-cell CAD model are required in order to tune the infinite slab properties within the desired frequency range. Nevertheless, in practical applications, the slab suffers from truncation effects and, especially for resonant inductive WPT, it is planned to be employed in the magnetic very near field region. Finally, the slab is also closely placed to a driver and a receiver coil, leading to strong interactions that must be considered. These practical aspects affect the metastructure response which will be inevitably different from what theoretically designed.

To overcome these limits, we propose for the first time a general analytical procedure to extract an accurate and unambiguous lumped parameters equivalent of a metasurface in resonant inductive WPT applications. The validity of the method is demonstrated through a test-case. We first design a classical WPT arrangement consisting in a fed loop (i.e., driving coil) and a passive receiver, both resonant at the same working frequency. In addition, we interpose a metasurface in between, exploiting the results coming from a single full-wave simulation to extract its equivalent *RLC* circuit and the mutual coupling coefficients with the driving and receiving coils. We demonstrate that the derived model is able to predict the behavior of the entire WPT setup for arbitrary vertical positions of the metasurface (i.e., the z-axis in Fig. 1), by comparing the 2-ports impedance matrix analytically calculated against full-wave simulations. The equivalent circuit model is able to fully describe not only the metasurface with its proper characteristics (such as the finiteness), but also the respective near-field interactions with a particular driver/receiver system. Moreover, it retains quantitative parameters to accomplish the design and the performance optimization of the specific WPT arrangement and the avoidance of a great number of computationally extensive full-wave simulations. Therefore, the metasurface design procedure can be easier and faster allowing a deeper advancement in the physical and practical understanding of the system.

This article is organized as follows. Section II presents the general analytical procedure for characterizing the metasurface starting from an initial full wave simulation, while in Section III practical design considerations are discussed. Section IV is devoted to verifying the proposed method applied to the test-case, comparing the model predictive performance against full-wave simulations and experimental measurements on a fabricated prototype. Finally, Conclusion follows.

II. METHODS

As introduced, metamaterials and metasurfaces are typically interposed between a driver and a receiver coil in WPT arrangements (Fig. 1). Their presence is fundamental to enhance the performance of the inductive link, increasing the efficiency and the useful working distance. Since they consist of arrays of resonant unit-cells, we consistently expect that their response to an impinging magnetic field shows a resonant behavior, as widely demonstrated in the open literature [16]–[18]. The specific aim of the present work is to explore the possibility of reducing an entire metasurface to a single equivalent *RLC* circuit interacting with the driver and receiver according to the schematic reported in Fig. 2.

Since the metasurface is a passive structure, we can acquire the 2-port impedance parameters (driver and receiver) to completely characterize the WPT system outlined in Fig. 1, according to the circuit model shown in Fig. 3. In particular, the 2-port model represented in Fig. 3 is valid in both cases, i.e., with and without the interposed passive metasurface. It is always possible to represent a 3-element circuit through its equivalent 2-port, by properly modifying the impedance terms Z_{ij}^{*}, as depicted in the inset of

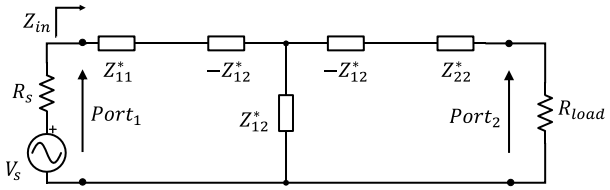

$$Z_{11}^* = Z_{11} - \frac{Z_{13}Z_{31}}{Z_{33}}$$
$$Z_{12}^* = Z_{12} - \frac{Z_{13}Z_{23}}{Z_{33}}$$
$$Z_{22}^* = Z_{22} - \frac{Z_{23}Z_{32}}{Z_{33}}$$

FIGURE 3. Schematic representation of the equivalent 2-port circuit describing the adopted WPT test case. In the presence of the metasurface, the impedance terms of port 1 and port 2 are modified according to the new values Z_{ij}^*.

Fig. 3 and shown later in Section II (for notation simplicity, we have indicated with the indexes 1, 2 and 3, the driver, the receiver and the passive metasurface, respectively). It may be worth noticing that the slab presence drastically changes the behavior of the mutual coupling between driver and receiver. Indeed, the Z_{21} parameter for a conventional configuration without the metasurface would be a classical inductive term: its insertion modifies this term, making it resonant with the appearance of an additional real component [36].

The possibility to have at disposal a single equivalent *RLC* circuit of a complex structure as a metasurface is important to predict the 2-port *Z*-parameters for different metasurface positions without resorting to full-wave simulations. Moreover, a lumped model is practically helpful since it allows quantifying and manipulating all the designing key parameters to obtain the desired properties for a given application. Such aspect overcomes the current limitation in WPT, i.e., the lack of practical design guidelines for the metasurface engineerization.

A. METASURFACE RLC EQUIVALENT CIRCUIT MODEL

Let us consider a WPT system consisting of a fed coil (i.e., the driver with its respective voltage source V_1) and a passive receiver, both resonant at the same working angular frequency ω_0. We also suppose to interpose in between a metasurface made up of an array of resonant unit-cells (Fig. 1).

If we refer to the driver with index 1, to the receiver with 2 and to the N elements of the array with $3, 4, \ldots N+2$, the overall system impedance matrix can be written as below.

$$\begin{pmatrix} Z_{11} & Z_{12} & Z_{13} & \ldots & Z_{1(N+2)} \\ Z_{21} & Z_{22} & Z_{23} & \ldots & Z_{2(N+2)} \\ Z_{31} & Z_{32} & Z_{33} & \ldots & Z_{3(N+2)} \\ \vdots & \vdots & \vdots & \vdots & \vdots \\ Z_{(N+2)1} & Z_{(N+2)2} & Z_{(N+2)3} & \ldots & Z_{(N+2)(N+2)} \end{pmatrix}$$

$$\begin{pmatrix} I_1 \\ I_2 \\ c_3 I_x \\ \vdots \\ c_{(N+2)} I_x \end{pmatrix} = \begin{pmatrix} V_1 \\ 0 \\ \vdots \\ 0 \\ 0 \end{pmatrix}, \tag{1}$$

in which we express the currents flowing in each element of the metasurface in the following form:

$$I_i = c_i I_x, \qquad with \;\; i = 3, 4, \ldots, N+2 \tag{2}$$

where c_i is the generic i-th complex current coefficient and I_x is the equivalent current. I_x has the precise physical meaning of representing the current flowing in the metasurface equivalent *RLC* which retains the same behavior of the whole array made of the N single resonators.

By summing up equations from row 3 to row $N+2$ and re-arranging terms, it is possible to write the following 3-coil system, where the N elements of the slab have been substituted by their equivalent resonator (marked with index x).

$$\begin{pmatrix} Z_{11} & Z_{12} & Z_{1x} \\ Z_{21} & Z_{22} & Z_{2x} \\ Z_{x1} & Z_{x2} & Z_{xx} \end{pmatrix} \begin{pmatrix} I_1 \\ I_2 \\ I_x \end{pmatrix} = \begin{pmatrix} V_1 \\ 0 \\ 0 \end{pmatrix}, \tag{3}$$

where:

$$\begin{cases} Z_{xx} = \sum_{i=3}^{N+2} \sum_{j=3}^{N+2} c_j Z_{ij} \\ Z_{x1} = \sum_{j=3}^{N+2} c_j Z_{1j} \\ Z_{x2} = \sum_{j=3}^{N+2} c_j Z_{2j} \end{cases} \tag{4}$$

We can notice that Z_{xx} can be interpreted as the self-impedance of the slab equivalent resonator (*RLC* series):

$$Z_{xx} = (R_x + j\omega L_x + 1/j\omega C_x) \tag{5}$$

The resonant frequency of the slab equivalent resonator is expressed by the following relation:

$$f_0 = \frac{1}{2\pi\sqrt{L_x C_x}} \tag{6}$$

At this point, we can apply the method also described in [9], and easily derive the resistance and the inductance of the equivalent resonator:

$$R_x = Re\{Z_{xx}\}, \tag{7}$$

whereas the inductance can be calculated from the following equation together with the knowledge of the resonant frequency of the overall slab ω_0 and the condition (6):

$$\begin{aligned} L_x &= \frac{1}{2}\frac{\partial}{\partial\omega}\{Im\{R_x + j\omega L_x + 1/j\omega C_x\}\}\Big|_{\omega=\omega_0} \\ &= \frac{1}{2}\frac{\partial}{\partial\omega}\{Im\{Z_{xx}\}\}\Big|_{\omega=\omega_0} \end{aligned} \tag{8}$$

Naturally, C_x follows from (6). Instead, the mutual coupling coefficients between the metasurface and the driver and between the slab and the receiver are, respectively:

$$\begin{cases} M_{x1} = \frac{Z_{x1}}{j\omega} \\ M_{x2} = \frac{Z_{x2}}{j\omega} \end{cases} \tag{9}$$

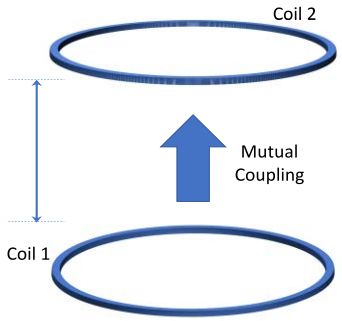

FIGURE 4. Schematic representation of the simple 2-loops test system used to estimate the mutual coupling dependence from distance.

In this way, we are able to characterize the equivalent *RLC* parameters of the array and the respective mutual coupling coefficients with the driver and the receiver.

Finally, it is worth highlighting that the equivalent metasurface Q-factor can be also derived:

$$Q = \frac{\omega_0 L_x}{R_x} = \frac{1}{R_x}\sqrt{\frac{L_x}{C_x}} \tag{10}$$

The Q-factor provides important information about the losses and the behavior of the slab as a whole, as it will be discussed later; thus, it can represent a synthetic parameter to evaluate the overall metasurface performance level.

B. METASURFACE RLC EQUIVALENT CIRCUIT EXTRACTION

In order to practically accomplish the metasurface equivalent circuit extraction, we need to perform a single full-wave simulation of a preliminary version of the investigated WPT system. The simulation provides the complete $(N+2)\times(N+2)$ impedance matrix (as reported in (1)) that is useful to derive the 3-coil system equivalent model, as described in the previous section. In addition, the 2-port impedance matrix, i.e., the system matrix of the circuit depicted in Fig. 3 (where only the ports at the driver and receiver are considered) can be also extracted from the simulation.

In particular, the system (3) can be rewritten to obtain the respective 2-port impedance matrix. Indeed, we can isolate the current I_x:

$$I_x = \frac{-Z_{x1}I_1 - Z_{x2}I_2}{Z_{xx}} \tag{11}$$

Substituting the expression of I_x in the other two equations of (3), we obtain the following equivalent 2-port system, which coincides with the 2-port impedance matrix directly evaluated through the numerical simulation.

$$\begin{pmatrix} Z_{11} - \frac{Z_{1x}Z_{x1}}{Z_{xx}} & Z_{12} - \frac{Z_{1x}Z_{2x}}{Z_{xx}} \\ Z_{21} - \frac{Z_{x2}Z_{x1}}{Z_{xx}} & Z_{22} - \frac{Z_{2x}Z_{x2}}{Z_{xx}} \end{pmatrix} \begin{pmatrix} I_1 \\ I_2 \end{pmatrix} = \begin{pmatrix} V_1 \\ 0 \end{pmatrix} \tag{12}$$

It is worth highlighting, as evident from (12), that each parameter of the 2-port full wave impedance matrix (i.e., the 2×2 matrix in (12)) exhibits a peak at the metasurface resonant frequency. The Z_{xx} parameter, being at the denominator, assumes the minimum value at the resonance (see (5)). Hence, it is easy to identify the resonant frequency f_0 from the *Z*-parameters obtained by the full-wave simulation and, consequently, retrieve the equivalent L_x andC_x from (6)–(8).

At this stage, the equivalent current I_x value is still arbitrary; through a least-square algorithm implemented in MATLAB (version R2019b), we identify I_x that minimizes the distance between the 2-port impedance parameters numerically simulated and those evaluated from (12), i.e., the ones calculated through the proposed equivalent model. In this way, the optimal *RLC* and mutual coefficients combination can be extracted.

In summary, the circuital equivalent retrieval steps are: *a*) perform a single full-wave simulation with the presence of the metasurface, extracting both the $(N+2)\times(N+2)$ and the 2×2 impedance matrix; *b*) reconstruct from (2), combined with (3) and (12), the 2-port parameters derived with the equivalent resonator; *c*) optimize the extracted lumped parameters by finding I_x that minimizes the distance between the 2×2 impedance parameters evaluated by the full-wave simulation and by the equivalent model (12).

C. MUTUAL COUPLING ESTIMATION

The usefulness of a model relies not only in its describing potential but also in its predictive value, i.e., the capability to predict the system performance without the need to carry out full-wave simulations.

In our specific case, for realizing a predictive equivalent model, we need the mutual coefficients M_{1x} and M_{2x} behavior when the slab position is changed. The equivalent model extraction procedure described in the previous sections is carried out for a fixed metasurface position but, whereas the *RLC* equivalent can be assumed to be an intrinsic property of the slab independent from its position, the mutual coupling is strictly dependent on it. Thus, our aim is finding the approximate dynamic of the mutual coupling when the metasurface is progressively moved from the driver towards the receiver.

It is well-known that the mutual inductance between two loops is dominated by their geometrical size and distance. One possibility to estimate the mutual coefficient dynamic with the distance is to calculate the coupling between two loops having a diameter within the same order of magnitude of the elements (driver, receiver and metasurface) of the considered WPT system (Fig. 4). Since the geometrical size are similar, the physical insight from this simpler situation can provide useful information also for the mutual coupling dynamic between driver/slab and receiver/slab.

Generally, inductive WPT is carried out at low frequency (∼few MHz); thus, we can apply the Biot-Savart formulation (magneto-static hypothesis) to estimate the mutual coupling between two generic loops [9]. Therefore, the magnetic field produced by a given current path in a specific point can be

expressed as:

$$\vec{B}(\vec{r}) = \frac{\mu_0}{4\pi} \int \frac{I\vec{dl} \times \vec{r'}}{\left|\vec{r'}\right|^3}, \tag{13}$$

where μ_0 (H/m) is the magnetic permeability of the vacuum, I (A) is the current amplitude flowing in the path, $\vec{dl}$ (m) is an infinitesimal element of the current path and $\vec{r'}$ (m) is the vector distance between the infinitesimal element $\vec{dl}$ and a generic point of the space (identified by $\vec{r}$). Then, the mutual coupling coefficient between the coils i and j is represented by the magnetic flux per unit current through the surface of coil j induced by the current flowing in coil i:

$$M_{ij} = \frac{\Phi_{ij}}{I_i}. \tag{14}$$

In this way, given the geometrical design of the two loops, we can numerically set a unit current flowing in one of them and evaluate the mutual inductive coupling with the other. This procedure – easy to calculate analytically – can be iterated for increasing distances between the two test loops, finding the general dynamic for the coupling as a function of the distance.

Since the mutual coupling between two coils is strictly dependent from their distance and from the available area for magnetic field concatenation, it is plausible to assume that the dynamic found for the two test-loops can be extended also for the couples driver/slab and receiver/slab. They share the same order of magnitude for the size and this guarantees that the available area for field concatenation is similar to the test-loops case. Hence, we can extrapolate the curves of the mutual coefficients M_{1x} and M_{2x} (slab-driver and slab-receiver) versus distance; we impose to the coupling coefficients M_{1x} and M_{2x} (obtained from the procedure reported in the previous sections for a precise fixed distance), the distance dynamic as estimated through the Biot-Savart law applied over the two test loops. At this stage, considering the procedure described in Section II-B and the mutual coupling estimation just described, we are able to completely define an equivalent circuit that allows fast and accurate simulation for a proper design of a WPT system with metasurface integration.

III. PRACTICAL DESIGN CONSIDERATIONS

As anticipated in the previous sections, the availability of an equivalent circuit model of a complex structure, like a metamaterial or metasurface, can be extremely useful to facilitate an effective design.

As it is well-known, the efficiency and the working distance are two of the most important parameters in a WPT application. They can be both improved through the driver-receiver inductive link strength maximization [18]. This can be practically translated into the Z_{12}^* enhancement, as described in Fig. 3; the metasurface effect on the Z_{11}^* and Z_{22}^* can be always compensated by appropriate technical solutions (matching networks or distance compensation). Hence, recalling (12), the following parameter has to be maximized:

$$Z_{21}^* = Z_{21} - \frac{Z_{x1}Z_{x2}}{Z_{xx}}. \tag{15}$$

In particular, the crucial term in (15) is the ratio on the right, which is related to the slab presence. At denominator, we find Z_{xx} given by equation (5); this term must present as low as possible resistive losses to increase the mutual coupling between driver and receiver. As shown in (4), the metasurface total losses can be directly obtained from the single unit-cells' self-resistances:

$$R_x = \sum_{i=3}^{N+2} c_i R_i \tag{16}$$

Resistive losses control is of outmost importance to enhance WPT performance; our model therefore suggests thick PCB copper traces or Litz-wire for metasurface fabrication [37].

Another important quantity to be considered for performance improvement is the ratio L_x/C_x. Since inductive resonant WPT is based on the magnetic field exchange between driving and receiving coils, a high L_x/C_x ratio ensures the slab capability to produce a significant magnetic field for a certain flowing current. As for R_x, also the total metasurface L_x can be obtained from the series of the unit-cells' inductances weighted by their respective current coefficient c_i:

$$L_x = \sum_{i=3}^{N+2} c_i L_i \tag{17}$$

This observation advises to pay particular attention to the unit-cell design, which must present a high inductance. Although various designs have been presented in the literature, one of the most convenient structure to achieve high inductance and compactness is the connected double-spiral resonator [17]. Another approach to increase the ratio L_x/C_x relies on the minimization of C_x. This can be achieved not only by L_x maximization, but also through the mutual coefficients Z_{ij} between unit-cells. For a typical planar configuration where unit-cells lay adjacent, the mutual coefficients Z_{ij} are purely reactive and negative [36]. Following (4), these mutual impedances are added, through their respective weights, in series with the single unit cells' capacitances, contributing to C_x. Thus, the higher the various mutual coefficients amplitude, the smaller the equivalent capacitor C_x. This suggests placing the unit-cells as close as possible (i.e., minimal periodicity) each other to enhance the magnetic response of the entire slab. It may be worth noticing that minimizing R_x and, simultaneously, maximizing the ratio L_x/C_x is globally equivalent to maximizing the Q-factor of the slab (10); the entire metasurface Q-factor can be considered as the most significative and synthetic parameter to evaluate the overall design effectiveness.

Finally, it is also important mentioning that we can also improve Z_{12}^* by increasing the numerator of the fraction at

the right of (15), i.e., by enhancing the mutual coefficients M_{x1} and M_{x2}. Inspired by (4), increasing the overall number of unit cells (and, consequently, the entire slab dimensions) may be considered a good choice to achieve this goal. Nevertheless, we should recognize that the contribution to the total mutual coupling M_{x1} and M_{x2} is very limited when the additional peripherical unit-cells are placed too far away from the driver and the receiver; conversely, their presence is detrimental because of the increase of resistive losses (16). It is fundamental choosing a compromise in the unit-cells number: when the M_{x1} and M_{x2} enhancement added by additional unit-cells is not able to compensate the supplementary losses (see (15)), it is appropriate to abstain from the metasurface enlargement.

All of these assessments can be highly facilitated by the equivalent circuit availability, since we can manipulate the key terms in a quantitative and straightforward manner. This approach reverses the classical metasurface design process, in which the infinite-extent slab properties are evaluated applying a plane-wave excitation and periodic boundary conditions on the unit-cell model to retrieve the respective equivalent permittivity and permeability. This classical method generally implies several iterations to optimize the unit-cell design, until the infinite slab shows the desired properties within the operative frequency range. Conversely, our method exploits an initial full-wave simulation of the entire actual system, i.e., the finite-extent metasurface with the particular driver and receiver coils arrangement. The derived circuital model allows to select the correct parameters to be modified to optimize the slab performance (unit-cells' inductance/capacitance, their periodicity, slab-driver relative position) in a direct manner. Moreover, the model fully considers the near-field regime at which the system operates as well as all the interactions between the metasurface and the particular RF coils arrangements. In this way, only few and targeted full-wave simulations have to be performed to optimize the system, since the herein provided guidelines can greatly help the designer to meet the required specifications.

IV. CASE STUDY

In order to validate the theoretical model described in the previous sections, we proposed the following WPT arrangement as a test-case (Fig. 5).

The design process and the numerical simulations were carried out by using an electromagnetic solver based on the Methods of Moments (Feko suite, Altair, Troy, MI, USA).

For simplicity, driver and receiver were realized as equal; they consisted of a 5-turn solenoid with 18 cm diameter, made up with 4 mm diameter lossy copper wire. They were also made resonant at around 6 MHz by adding a capacitive load of 81 pF. The working frequency has been chosen within the typical range for WPT devices. Finally, driver and receiver were coaxially placed at 18 cm distance. Then, we inserted between them a metasurface, constituted by a 5×5 array. As explained in the previous section, the array dimension can be generally chosen considering that the

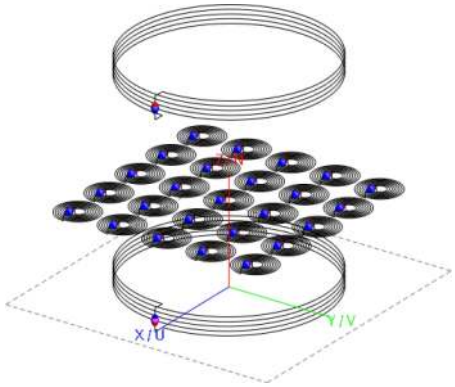

FIGURE 5. 3D CAD model of the proposed WPT arrangement.

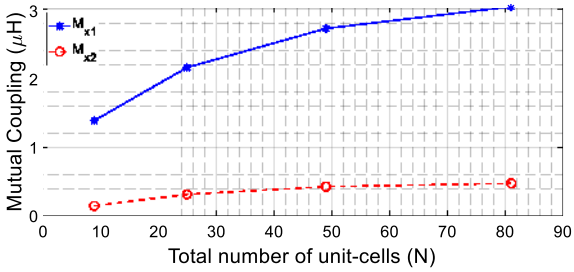

FIGURE 6. The mutual coupling coefficients between driver-metasurface and receiver-metasurface increase slower with an increasing number of unit-cells *N*. The values of the coefficients are extracted for a driver-metamaterial distance of 2 cm.

contribution of additional unit-cells to the mutual coupling coefficients M_{x1} and M_{x2} is less and less pronounced (Fig. 6), while the resistive term increases linearly with the unit-cells number N. Each unit-cell was designed as a 8-turn planar spiral with an inner diameter of 1 cm and external size of 4 cm, with two adjacent branches separated by 0.6 mm. The unit-cells are placed 3 mm away from the closest neighbors. In this case, a 1.4 mm diameter lossy copper wire was chosen as material. The cells were loaded with 585 pF capacitors that allowed the entire slab to resonate at 6 MHz.

Finally, in order to simulate a typical WPT arrangement, we also added a series resistance of 50 Ω to the driver (to represent the output impedance of a power amplifier [17]) and an useful 50 Ω series load at the receiver. The metasurface was initially placed 1.5 cm away from the driver.

A. FULL-WAVE SIMULATIONS: RLC EXTRACTION

The first step consisted in the metasurface *RLC* extraction; with this aim, we placed the slab 1.5 cm away from the driver, but also other positions could have been adopted. We run a single full-wave simulation at the chosen working frequency (6.12 MHz), imposing a 1 V voltage source at the driver and evaluating the system impedance matrix and the current amplitude in every array element of the designed metasurface.

Following the procedure described in the previous section, we extracted the full impedance matrix (27×27), reducing it to its 3×3 equivalent (3). From this 3×3 system, we recovered the 2×2 impedance matrix applying the transformation

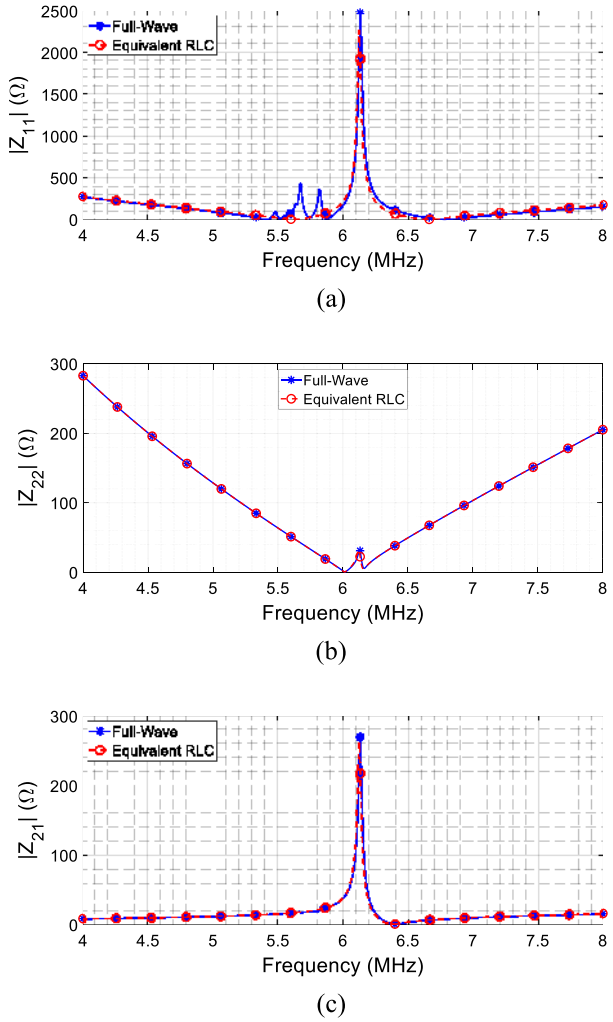

FIGURE 7. Comparison between the 2-port impedance parameters obtained from full-wave simulations and from the extraction analytical model. (a) Z_{11}^*, (b) Z_{22}^*, (c) Z_{21}^*. The good agreement can be highlighted.

described in (12). We then compared these impedance parameters with the 2-port (driver and receiver) impedance matrix directly obtained from the full-wave simulation. Finally, we evaluated the slab *RLC* and its mutual coefficients with the driver and receiver by finding the equivalent current I_x that led to the best matching between the model and the simulation. This value resulted in 7.05 mA considering the 1 V voltage source at the driving coil. The obtained metasurface equivalent lumped parameters were: $R_x = 4.92\Omega$, $L_x = 30.2\mu$H, $C_x = 22.3$ pF, $M_{1x} = 2.74\mu$H, $M_{2x} = 0.32\mu$H (index 1 is referred to the driver, index 2 to the receiver). The slab Q-factor resulted in 236.9.

In summary, we achieved an excellent agreement between the full-wave simulated and the equivalent extracted 2-port impedance parameters (Fig. 7). This demonstrates that the developed analytical model guarantees a high degree of fidelity and can be considered as the actual equivalent circuit of a metasurface. As a matter of fact, we have to consider a certain degree of approximation with the proposed model;

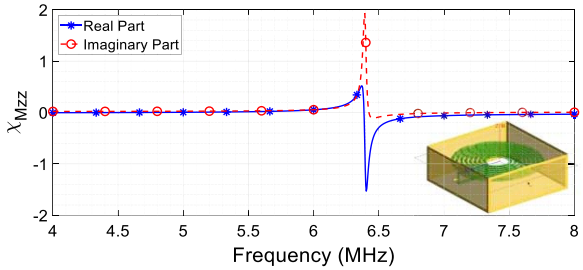

FIGURE 8. Retrieved superficial magnetic susceptibility (Real and Imaginary components), orthogonal to the slab plane: as evident, the resonance is predicted for a different value w.r.t. the circuital model, because the slab finiteness and its interactions with driving and receiving coils are not considered. *Inset*: CAD model with periodic boundary conditions developed in Feko to perform the classical metasurface characterization [38].

all the secondary phenomena happening in the system, as for instance spurious resonances (evident from the Z_{11}^* parameter ripples, Fig. 7 (a)), cannot be properly followed.

In order to show the improvement of the circuit model here derived, we also performed the conventional metasurface characterization for the infinite-extent case and with a plane wave impinging on the structure in sub-wavelength regime.

We followed the theory developed by Holloway *et al.* [38], that was demonstrated to be the most formally correct to describe a thin meta-structure. The simulation model (with the periodic boundary conditions) and the relative graph about the superficial magnetic susceptibility (orthogonal to the slab plane) are reported in Fig. 8. As it can be seen, we can distinguish a negative susceptibility region after the resonance, as expected. The negative values of the imaginary part after the resonance point can be attributed to the intrinsic ambiguity in this extraction method [39]. Moreover, the overall resonance of the metasurface happens at 6.4 MHz, which is different from the actual slab resonance (at 6.12 MHZ, as evident from Fig. 7). The reason for this is that the classical theoretical model does not consider the finite dimension of the slab nor its interactions with the actual driver and receiver. On the other hand, our equivalent circuit model incorporates all of these aspects; hence, it can be useful to predict the correct behavior of the metasurface itself and in combination with the particular coils' arrangement. Differently from the conventional characterization procedure, we are able to precisely predict the input impedance at the driver/receiver ports and to optimize the metasurface design and size all at once; consequently, we can obtain the best performance for a given set-up, as already reported in Section III.

B. MUTUAL COUPLING EXTRACTION

As previously mentioned, the possibility to predict the impedance parameters of the WPT system for different positions of the metasurface without resorting to full-wave simulations is an important step in order to simplify the optimization of a given set-up and to grasp a physical meaning of the interactions between the various system components.

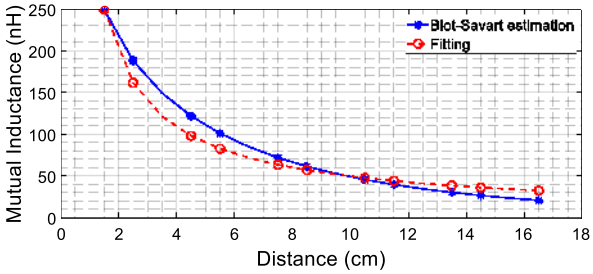

(a)

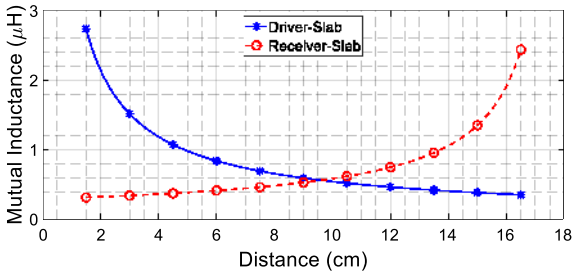

(b)

FIGURE 9. (a) Mutual inductance between the two test-loops versus their separation distance; the curve can be fitted with a $1/d^{0.85}$ behavior. (b) Extrapolated mutual coefficients M_{1x} and M_{2x}; starting from the coefficients values extracted through the proposed procedure, we hypothesized for them the same dynamic with the slab-driver separation distance observed between the test-loops.

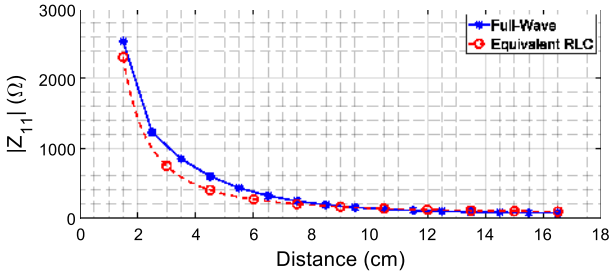

(a)

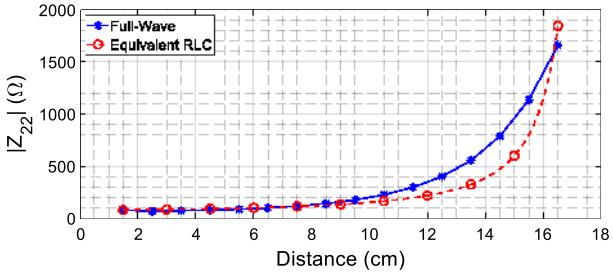

(b)

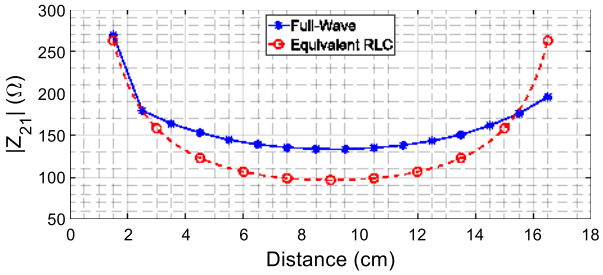

(c)

FIGURE 10. Model-predicted and full-wave 2-port impedance parameters comparison at the working frequency (6 MHz). Z_{11}^* (a), Z_{22}^* (b) and Z_{21}^* (c) are reported in absolute values for different metasurface axial positions (distances are w.r.t. the driver coil). An overall good agreement can be observed.

Following the theoretical analysis developed in Section II-C, the first step to estimate the dynamic versus distance of the mutual coefficients M_{1x} and M_{2x} (slab/driver and slab/receiver) requires evaluating the mutual induction behavior between two test-loops sharing the same order dimensions of the elements of the adopted WPT system. We assumed, as usual for metasurfaces in WPT, that driver, slab and receiver are coaxially placed. Only vertical shift of the metasurface has been considered. Therefore, we took into account two identical test-loops with a 10 cm radius, separated by a gap ranging from 1.5 to 16.5 cm (Fig. 4). This gap range coincides with the available space between the designed driver and receiver in our WPT set-up. In Fig. 9(a) we reported the mutual coupling dynamic between these two test-loops; the results show that the Biot-Savart estimation can be matched by a $1/d^{0.85}$ law. We adopted this law also for the mutual coefficients M_{1x} and M_{2x}, extracted as described in the previous section for a metasurface-driver distance of 1.5 cm. Fig. 9(b) shows the respective extrapolated values.

C. MODEL PREDICTIONS FOR DIFFERENT SLAB-DRIVER DISTANCES

Afterwards, we tested the predictive value of our equivalent model for different axial positions of the interposed metasurface. We evaluated the WPT arrangement by progressively placing the slab from 1.5 cm to 16.5 cm away from the driver (and vice versa with respect to the receiver) with 1 cm steps.

First, we analytically calculated for each slab position the 2-port impedance matrix as described in (12), using the extracted *RLC* equivalent parameters (reported in Section IV-A) and the mutual coefficient M_{1x} and M_{2x} as depicted in Fig. 9(b). Then, we compared the 2-port impedance parameters absolute values retrieved through the analytical model with the respective full-wave simulations. Fig. 10 shows the obtained results: we evaluated the Z_{11}^*, Z_{22}^* and Z_{21}^* in their absolute values and at the working frequency of the system (6 MHz). As evident, our model is able to predict with a good agreement the full-wave impedance matrix, thus demonstrating itself effective to reduce the computational burden and to facilitate the design and the optimization of the WPT systems with the presence of metamaterials and metasurfaces.

D. EXPERIMENTAL RESULTS

We also fabricated a prototype of the WPT system described in Section IV to validate experimentally the extracted slab lumped model. Specifically, we realized driver and receiver as two identical solenoids with 5 turns, made with 4 mm

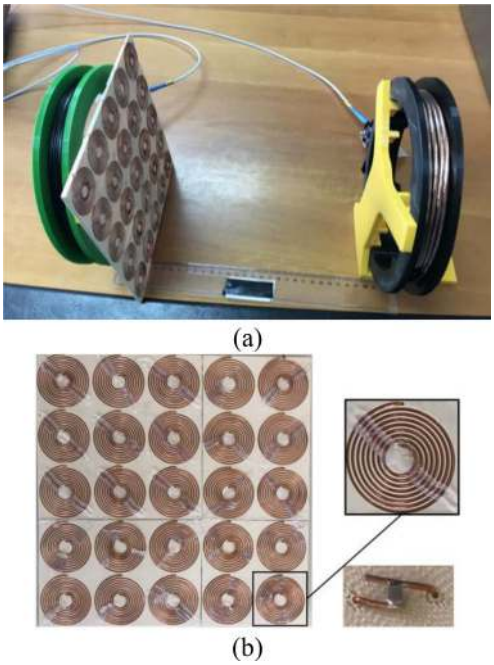

FIGURE 11. (a) Fabricated WPT system (as numerically designed). (b) Zoomed view of the metamaterial slab prototype (b).

diameter Litz wire. As reported in the numerical set-up, we equipped the two coils with a 81 pF capacitor to obtain the resonant frequency at about 6 MHz (Fig. 11 (a)). Then, the metasurface was fabricated, as a 5×5 matrix of resonant planar spiral resonators, with the same geometrical constraints reported in the design section.

The unit-cells were realized with a single strand 1.4 mm diameter copper wire, exploiting the grooves directly engraved onto a 5 mm thick PLA slab through 3D printing (Fig. 11 (b)). Each unit-cell was made resonant at the desired frequency by adding a 560 pF capacitor. We placed the metasurface 1.5 cm away from the driver and 16.5 cm far from the receiver, in a coaxial fashion (as reported in the numerical model). The 2-port (driver-receiver) Z-parameters were acquired with and without the metasurface through VNA (Keysight E5071C-ENA). In particular, we compared the 2-port impedance matrix when the system includes the slab with the matrix reconstructed using the experimental measurements acquired without the slab in combination with the lumped values extracted in the characterization step ($R_x = 4.92\Omega$, $L_x = 30.2\mu$H, $C_x = 22.3$ pF, $M_{1x} = 2.74\mu$H, $M_{2x} = 0.32\mu$H). The 2-port Z-matrix reconstruction was accomplished exploiting the relations described in (12).

Fig. 12 reports the obtained results; we can observe a very good agreement between the two cases, i.e., the measured full system (driver-slab-receiver) and the model-retrieved system (i.e., using the driver-receiver measurements in combination with the extracted lumped model). Such results demonstrate the accuracy and reliability of the proposed procedure in extracting the metasurface equivalent lumped circuit. The slight resonant frequency shift between the model case and the measurements can be mainly addressed to imperfections of fabrication and capacitance tolerances.

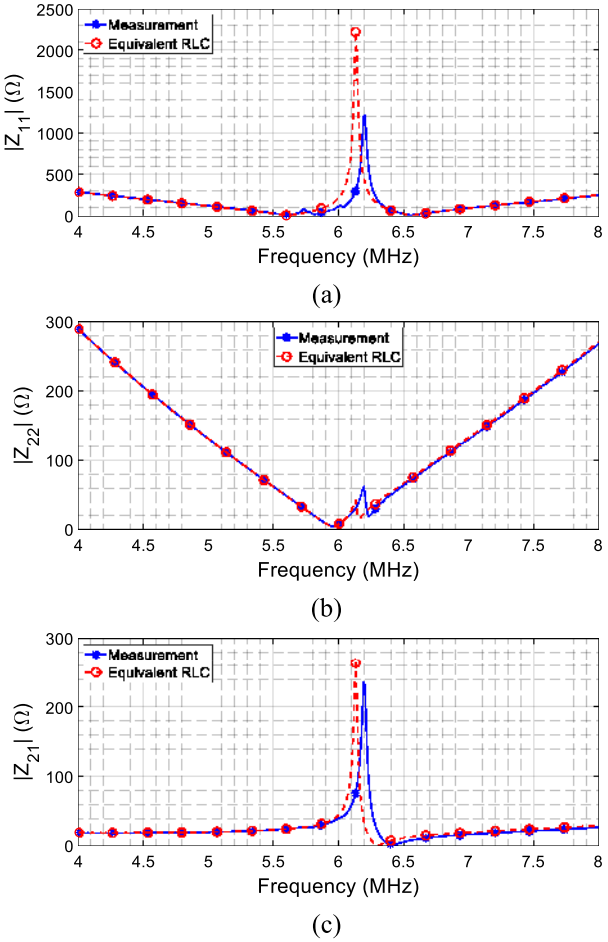

FIGURE 12. Comparison between the 2-port impedance parameters obtained from measurements on the full WPT system (driver-slab-receiver) and from the measurements on the driver-receiver only system in combination with the extracted slab lumped model. (a) Z^*_{11}, (b) Z^*_{22}, (c) Z^*_{21}. The excellent agreement can be highlighted.

V. CONCLUSION

In this article, we introduced a general analytical procedure to extract a lumped parameters circuital equivalent for metamaterials and metasurfaces employed in resonant inductive Wireless Power Transfer applications.

We proved through full-wave simulations that our analytical procedure is extremely accurate to achieve a reliable *RLC* equivalent circuit and, in addition, it provides quantitative and manageable parameters to predict and improve the entire WPT system performance. Furthermore, the numerical results have been validated through experimental measurements performed over a fabricated prototype. The extraction procedure exploits only a single full-wave simulation to retrieve the lumped model of the slab, avoiding several additional computationally expensive and time-consuming numerical simulations to optimize the performance of the WPT system. Naturally, having at disposal an effective

lumped equivalent circuit of a complex structure – like metamaterials and metasurfaces – can be extremely important to grasp a fundamental physical meaning of its different interactions with driving and receiving coils, and to consider both the inevitable truncation effects and the WPT near-field operative region. These practical aspects make our model more accurate and effective for WPT metasurface design with respect to the conventional sub-wavelength homogenization theories. Therefore, general guidelines based on the circuit model here presented have been provided, which can greatly help the designer to perfectionate the metasurface prototype according to the project specifications.

In conclusion, the obtained results can pave the way to a simpler and more effective approach to metamaterials and metasurfaces in resonant inductive WPT, significantly improving the design process and facilitating the adoption of these structures in practical applications. Future developments will be directed to a more accurate circuital modelization, aiming to describe also higher order resonances due to the elementary interactions between unit-cells.

REFERENCES

[1] S. B. Glybovski, S. A. Tretyakov, P. A. Belov, Y. S. Kivshar, and C. R. Simovski, "Metasurfaces: From microwaves to visible," *Phys. Rep.*, vol. 634, pp. 1–72, May 2016.

[2] A. Sihvola, "Metamaterials in electromagnetics," *Metamaterials*, vol. 1, no. 1, pp. 2–11, Mar. 2007, doi: 10.1016/j.metmat.2007.02.003.

[3] S. A. Tretyakov, "Complex-media electromagnetics and metamaterials," *J. Opt.*, vol. 19, no. 8, Jul. 2017, Art. no. 084006, doi: 10.1088/2040-8986/aa7956.

[4] D. R. Smith, J. B. Pendry, and M. C. Wiltshire, "Metamaterials and negative refractive index," *Science*, vol. 305, no. 5685, pp. 788–792, 2004.

[5] J. B. Pendry, "Negative refraction makes a perfect lens," *Phys. Rev. Lett.*, vol. 85, no. 18, p. 3966, 2000.

[6] J. Pendry, "Manipulating the near field with metamaterials," *Opt. Photon. News*, vol. 15, no. 9, pp. 32–37, 2004.

[7] F. Costa, A. Monorchio, and G. Manara, "Efficient analysis of frequency-selective surfaces by a simple equivalent-circuit model," *IEEE Antennas Propag. Mag.*, vol. 54, no. 4, pp. 35–48, Aug. 2012, doi: 10.1109/MAP.2012.6309153.

[8] F. Costa, S. Genovesi, A. Monorchio, and G. Manara, "A circuit-based model for the interpretation of perfect metamaterial absorbers," *IEEE Trans. Antennas Propag.*, vol. 61, no. 3, pp. 1201–1209, Mar. 2013, doi: 10.1109/TAP.2012.2227923.

[9] D. Brizi, N. Fontana, F. Costa, and A. Monorchio, "Accurate extraction of equivalent circuit parameters of spiral resonators for the design of metamaterials," *IEEE Trans. Microw. Theory Techn.*, vol. 67, no. 2, pp. 626–633, Feb. 2019, doi: 10.1109/TMTT.2018.2883036.

[10] F. Bilotti, A. Toscano, L. Vegni, K. Aydin, K. B. Alici, and E. Ozbay, "Equivalent-circuit models for the design of metamaterials based on artificial magnetic inclusions," *IEEE Trans. Microw. Theory Techn.*, vol. 55, no. 12, pp. 2865–2873, Dec. 2007.

[11] K. B. Alici, F. Bilotti, L. Vegni, and E. Ozbay, "Optimization and tunability of deep subwavelength resonators for metamaterial applications: Complete enhanced transmission through a subwavelength aperture," *Opt. Exp.*, vol. 17, no. 8, pp. 5933–5943, 2009.

[12] C. R. Simovski, "Bloch material parameters of magneto-dielectric metamaterials and the concept of Bloch lattices," *Metamaterials*, vol. 1, no. 2, pp. 62–80, 2007.

[13] A. Alu, "First-principles homogenization theory for periodic metamaterials," *Phys. Rev. B*, vol. 84, no. 7, 2011, Art. no. 075153.

[14] D. R. Smith and J. B. Pendry, "Homogenization of metamaterials by field averaging," *J. Opt. Soc. Amer. B*, vol. 23, no. 3, pp. 391–403, 2006.

[15] M. G. Silveirinha, "Metamaterial homogenization approach with application to the characterization of microstructured composites with negative parameters," *Phys. Rev. B*, vol. 75, no. 11, 2007, Art. no. 115104.

[16] A. Rajagopalan, A. K. RamRakhyani, D. Schurig, and G. Lazzi, "Improving power transfer efficiency of a short-range telemetry system using compact metamaterials," *IEEE Trans. Microw. Theory Techn.*, vol. 62, no. 4, pp. 947–955, Apr. 2014.

[17] D. Brizi, J. P. Stang, A. Monorchio, and G. Lazzi, "A compact magnetically dispersive surface for low-frequency wireless power transfer applications," *IEEE Trans. Antennas Propag.*, vol. 68, no. 3, pp. 1887–1895, Mar. 2020, doi: 10.1109/TAP.2020.2967320.

[18] E. S. G. Rodríguez, A. K. RamRakhyani, D. Schurig, and G. Lazzi, "Compact low-frequency metamaterial design for wireless power transfer efficiency enhancement," *IEEE Trans. Microw. Theory Techn.*, vol. 64, no. 5, pp. 1644–1654, May 2016.

[19] Y. Zhao, V. Vutipongsatorn, and E. Leelarasmee, "Improving the efficiency of wireless power transfer systems using metamaterials," in *Proc. 10th Int. Conf. Elect. Eng./Electron. Comput. Telecommun. Inf. Technol. (ECTI-CON)*, Krabi, Thailand, 2013, pp. 1–4.

[20] A. Grbic and G. V. Eleftheriades, "Growing evanescent waves in negative-refractive-index transmission-line media," *Appl. Phys. Lett.*, vol. 82, no. 12, pp. 1815–1817, Mar. 2003, doi: 10.1063/1.1561167.

[21] J. Choi and C. Seo, "High-efficiency wireless energy transmission using magnetic resonance based on negative refractive index metamaterial," *Progr. Electromagn. Res.*, vol. 106, pp. 33–47, Jan. 2010.

[22] Y. Urzhumov and D. R. Smith, "Metamaterial-enhanced coupling between magnetic dipoles for efficient wireless power transfer," *Phys. Rev. B*, vol. 83, no. 20, May 2011, Art. no. 205114, doi: 10.1103/PhysRevB.83.205114.

[23] J.-F. Chen *et al.*, "Metamaterial-based high-efficiency wireless power transfer system at 13.56 MHz for low power applications," *Progr. Electromagn. Res.*, vol. 72, pp. 17–30, Jan. 2017.

[24] T. Shaw, A. Roy, and D. Mitra, "Efficiency enhancement of wireless power transfer system using MNZ metamaterials," *Progr. Electromagn. Res.*, vol. 68, pp. 11–19, Jan. 2016.

[25] Z. Zhang, B. Zhang, B. Deng, X. Wei, and J. Wang, "Opportunities and challenges of metamaterial-based wireless power transfer for electric vehicles," *Wireless Power Transf.*, vol. 5, no. 01, pp. 9–19, Mar. 2018, doi: 10.1017/wpt.2017.12.

[26] K. Chen and Z. Zhao, "Analysis of the double-layer printed spiral coil for wireless power transfer," *IEEE J. Emerg. Sel. Topics Power Electron.*, vol. 1, no. 2, pp. 114–121, Jun. 2013, doi: 10.1109/JESTPE.2013.2272696.

[27] W.-C. Chen, C. M. Bingham, K. M. Mak, N. W. Caira, and W. J. Padilla, "Extremely subwavelength planar magnetic metamaterials," *Phys. Rev. B*, vol. 85, no. 20, May 2012, Art. no. 201104(R), doi: 10.1103/PhysRevB.85.201104.

[28] B. Wang, K. H. Teo, T. Nishino, W. Yerazunis, J. Barnwell, and J. Zhang, "Experiments on wireless power transfer with metamaterials," *Appl. Phys. Lett.*, vol. 98, no. 25, Jun. 2011, Art. no. 254101, doi: 10.1063/1.3601927.

[29] A. L. A. K. Ranaweera, T. P. Duong, and J.-W. Lee, "Experimental investigation of compact metamaterial for high efficiency mid-range wireless power transfer applications," *J. Appl. Phys.*, vol. 116, no. 4, Jul. 2014, Art. no. 043914, doi: 10.1063/1.4891715.

[30] H. Zhu, X. Luo, C. Zhao, Z. Hong, and Z. Huang, "Design and optimization of deep sub-wavelength metamaterials using a hybrid search algorithm," in *Proc. IEEE Wireless Power Trans. Conf. (WPTC)*, Taipei, Taiwan, 2017, pp. 1–4.

[31] Y. Cho *et al.*, "Thin hybrid metamaterial slab with negative and zero permeability for high efficiency and low electromagnetic field in wireless power transfer systems," *IEEE Trans. Electromagn. Compat.*, vol. 60, no. 4, pp. 1001–1009, Aug. 2018, doi: 10.1109/TEMC.2017.2751595.

[32] D. C. Corrêa, U. C. Resende, and F. S. Bicalho, "Experiments with a compact wireless power transfer system using strongly coupled magnetic resonance and metamaterials," *IEEE Trans. Magn.*, vol. 55, no. 8, pp. 1–4, Aug. 2019.

[33] H. An, G. Liu, Y. Li, J. Song, C. Zhang, and M. Liu, "Inhomogeneous electromagnetic metamaterial design method for improving efficiency and range of wireless power transfer," *IET Microw. Antennas Propag.*, vol. 13, no. 12, pp. 2110–2118, Oct. 2019.

[34] D. Brizi, N. Fontana, M. Tucci, S. Barmada, and A. Monorchio, "A spiral resonators passive array for inductive wireless power transfer applications with low exposure to near electric field," *IEEE Trans. Electromagn. Compat.*, vol. 62, no. 4, pp. 1312–1322, Aug. 2020, doi: 10.1109/TEMC.2020.2991123.
[35] T. Shaw and D. Mitra, "Metasurface-based radiative near-field wireless power transfer system for implantable medical devices," *IET Microw. Antennas Propag.*, vol. 13, no. 12, pp. 1974–1982, Oct. 2019.
[36] D. Brizi *et al.*, "Design of distributed spiral resonators for the decoupling of MRI double-tuned RF coils," *IEEE Trans. Biomed. Eng.*, vol. 67, no. 10, pp. 2806–2816, Oct. 2020, doi: 10.1109/TBME.2020.2971843.
[37] G. Giovannetti, N. Fontana, A. Monorchio, M. Tosetti, and G. Tiberi, "Estimation of losses in strip and circular wire conductors of radiofrequency planar surface coil by using the finite element method," *Concepts Magn. Reson. B, Magn. Reson. Eng.*, vol. 47B, no. 3, 2017, Art. no. e21358, doi: 10.1002/cmr.b.21358.
[38] C. L. Holloway, E. F. Kuester, J. A. Gordon, J. O'Hara, J. Booth, and D. R. Smith, "An overview of the theory and applications of metasurfaces: The two-dimensional equivalents of metamaterials," *IEEE Antennas Propag. Mag.*, vol. 54, no. 2, pp. 10–35, Apr. 2012.
[39] S. Arslanagić *et al.*, "A review of the scattering-parameter extraction method with clarification of ambiguity issues in relation to metamaterial homogenization," *IEEE Antennas Propag. Mag.*, vol. 55, no. 2, pp. 91–106, Apr. 2013, doi: 10.1109/MAP.2013.6529320.

DANILO BRIZI (Member, IEEE) was born in Viterbo, Italy, in 1992. He received the M.S. Laurea degree (*summa cum laude*) in biomedical engineering and the Ph.D. degree in information engineering from the University of Pisa in 2016 and 2020, respectively, where he is currently working as a Postdoctoral Researcher. His research interests include hyperthermia with magnetic nanoparticles, MRI filter design, and wireless power transfer applications.

NUNZIA FONTANA (Member, IEEE) was born in Agrigento, Italy, in 1984. She received the M.Sc. degree (*summa cum laude*) in telecommunications engineering and the Ph.D. degree in remote sensing from the University of Pisa, Italy, in 2008 and 2012, respectively, where she was a Postdoctoral Researcher from 2012 to 2016. From 2016 to 2019, she was a Researcher with the National Inter-University Consortium for Telecommunications. She is currently an Assistant Professor with the Department of Energy, Systems, Territory and Construction Engineering, University of Pisa. Her research activities have been published in several international scientific journals and in a number of international conference proceedings. Her research interests include: wireless power transfer; antennas, impedance matching networks design, prototyping and RF testing; radio frequency coils design for magnetic resonance and RF testing; and bio-electromagnetics. She serves as an Associate Editor for *ACES Journal*. She is a member of ACES.

SAMI BARMADA (Senior Member, IEEE) received the M.S. and Ph.D. degrees in electrical engineering from the University of Pisa, Italy, in 1995 and 2001, respectively.

He is currently a Full Professor with the Department of Energy and System Engineering, University of Pisa. He has authored and coauthored more than 120 papers in international journals and indexed conferences. His research interests include applied electromagnetics, electromagnetic fields calculation, power line communications, wireless power transfer devices, and nondestructive testing. He is a member of the International Steering Committee of the CEFC Conference and he has been the general chairman and a technical program chairman of numerous international conferences. He is an Applied Computational Electromagnetics Society (ACES) Fellow and he served as an ACES President from 2015 to 2017.

AGOSTINO MONORCHIO (Fellow, IEEE) is a Full Professor with the University of Pisa. He spent several research periods with the Electromagnetic Communication Laboratory, Pennsylvania State University, USA, both as a recipient of a Scholarship (Fellowship Award) of the Summa Foundation, Albuquerque, NM, USA, and in the framework of CNR-NATO Senior Fellowship Programme. He has carried out a considerable research activity and technical consultancy to national, EU and U.S. industries, coordinating, as a Principal Scientific Investigator, a large number of national and European research projects. He is active in a number of areas, including computational electromagnetics, microwave metamaterials, radio propagation for wireless systems, the design and miniaturization of antennas and electromagnetic compatibility, and biomedical microwaves applications. The activity is mainly carried out with the Microwave and Radiation Laboratory (www.mrlab.it), Department of Information Engineering, University of Pisa, together with a large group of Ph.D. students, Postdoctorals, and Research Associates. He has coauthored four patents. His research results have been published in more than 130 journal papers and book chapters, and more than 200 communications at international and national conferences.

He serves as a reviewer for international journals, and he was an Associate Editor of IEEE ANTENNAS AND WIRELESS PROPAGATION LETTERS from 2002 to 2007. He has been an AdCom Member from 2017 to 2019 and he is a Co-Chair of the Industrial Initiative Committee of the IEEE APS. He is a member of RaSS National Laboratory, Consorzio Nazionale Interuniversitario per le Telecomunicazioni, and in 2010 he affiliated with the Pisa Section of INFN, the National Institute of Nuclear Physics. In 2012, he has been elevated to Fellow grade by the IEEE for his contributions to computational electromagnetics and for application of frequency selective surfaces in metamaterials.